

ACTIVE REGION FLOWS

Peter Foukal
Cambridge Research and Instrumentation, Inc.
Cambridge, Massachusetts

Abstract

A wide range of observations has shown that active region phenomena in the photospheric, chromospheric and coronal temperature regimes are dynamical in nature. We focus here on three topics where substantial developments have occurred in the past few years. At the photosphere, recent observations of full line profiles place an upper limit of about $+20 \text{ msec}^{-1}$ on any downflows at supergranule cell edges. Observations of the full Stokes V profiles in the network show no evidence for downflows in magnetic flux tubes either, although the errors here are still an order of magnitude larger. Velocity observations such as those planned with HRSO can be designed to avoid the spurious signals generated by line profile changes.

In the area of chromospheric dynamics, several models have been put forward recently to reproduce the observed behavior of spicules. However, we point out that these adiabatic models do not include the powerful radiative dissipation which tend to damp out the large-amplitude disturbances that produce the spicular acceleration in the models. HRSO observations would be helpful in tracing spicule development from the triggering process through evolution of the structure, and thus help to decide whether much longer-period photospheric disturbances or spicule triggering at much higher altitudes might avoid the dissipation and produce more promising results.

In the corona, loop flows along field lines clearly transport mass and energy at rates important for the dynamics of these structures. However, advances in understanding the heating and mass balance of the loop structures seem to require new kinds of observations. We present some results using a remote sensing diagnostic of the intensity and orientation of macroscopic plasma electric fields predicted by models of reconnective heating and also wave heating. Use of this diagnostic should be possible from HRSO with significantly higher spatial resolution and sensitivity than is possible from the ground.

PRECEDING PAGE BLANK NOT FILMED

I. Introduction

We have seen many fine space- and ground-based observations presented at this meeting. It is probably useful to show an old observation to remind us that the subject of flows in active regions, and their control by electromagnetic forces, is quite venerable. Figure 1 is a drawing made of an active region at the limb in H_{α} by A. Secchi on October 5, 1871. This drawing, made from visual observations through a spectrohelioscope, shows most of the basic structures we are still seeking to understand--a well-defined loop system, coronal rain, spicules and some surging activity. This illustrates a point which has been made also in several of the preceding papers, that interpretation is lagging rather far behind observations.

The remedy is of course not to stop observing--understanding can come only from much better data of the kind that we expect from HRSO. But we do perhaps need to think more clearly about the specific observations that are required to answer some rather long-standing and relatively well-posed problems.

II. Overview of Active Region Flows

Figure 2 shows schematically some of the basic types of flows that have been identified in active regions (see, e.g., review by Athay 1981). Associated with spots we find the strong Evershed flows of the penumbra, and in the H_{α} superpenumbra that overlies it, a predominant inflow. Evidence on the Evershed outflow indicates it is confined to dark penumbral filaments of relatively low magnetic field strength (see review by Moore 1981). It is not yet clear whether it represents a steady outward flow or whether it reverses within individual filaments on time scales comparable to the penumbral crossing time and returns along less visible paths. Within spots, one finds a relatively static atmosphere, with no detectable large-scale flow (Beckers 1977). In the corona above the spot we observe predominantly downflowing material, "coronal rain," not only in H_{α} , but also in the EUV radiations (Foukal 1978, Brueckner 1981).

The excellent HRTS rocket and Spacelab data also give us our best look at flows in coronal radiations, which consist of up and downflows over spots and plages at velocities around 30 km sec^{-1} (Brueckner 1981). Analysis of the Skylab EUV data showed rapid variations in the intensities of plasma radiations, which have been interpreted as explosive bursts (Emslie and Noyes 1978). In the chromosphere we have many observations of spicules and fibrils in visible radiations (see review by Beckers 1972) and now also in the ultraviolet (Cook 1985).

Lower in the atmosphere, there has been much work on flows in and around magnetic flux tubes ever since the report of systematic redshifts in network boundaries by Simon and Leighton (1964), and the later report of strong downdrafts within the small network flux tubes by Giovanelli and Slaughter (1978). The relative motions of photospheric flux tubes are in themselves tracers of velocity fields at deeper layers (see, e.g., review by Gilman and Foukal 1979).

Since there isn't time to discuss all of the above flow phenomena, I would like to concentrate on three topics where interesting progress has been made in observations and theory. One area is the observational evidence on photospheric flows inside and around flux tubes, and their relation to the

supergranulation. Another is the dynamics of spicules and fibrils. Finally, I would like to present some new observational evidence with a direct bearing on the dynamics of coronal flows in magnetic loops.

III. Photospheric Flows at Supergranule Boundaries and Within Flux Tubes

The observations of the supergranular flow pattern obtained by Simon and Leighton (1964) led to the concept of an overturning supergranular convective cell. Strong horizontal flows $v_h \sim 0.5 \text{ km sec}^{-1}$ are observed to diverge from the cell center. No good evidence has ever been given for any significant upflow velocity $v_u \gtrsim 10 \text{ msec}^{-1}$ (Giovanelli 1980). However, relatively strong redshifts near the flow edges were interpreted as downflows of amplitude 100-200 msec^{-1} . The correlation between network (marked by excess brightness in Fraunhofer lines) and redshifts is well illustrated by Tanenbaum et al. (1969).

Observations by Howard (1972) and others showed that systematic redshifts over network and faculae were observed whenever a magnetograph Doppler servo was used to measure photospheric velocities. The large areas covered by these apparent downdrafts and the absence of any detectable compensating blue-shifted material led to the increasing suspicion that at least a large part of the redshift was generated by magnetic suppression of the blue-shift of Fraunhofer lines. This blue-shift near disc center is known to be caused by the intensity-velocity correlation of granules (see review by Dravins, Lindegren and Nordlund 1981). Somewhat surprisingly, the observations of full line profiles at cell centers and boundaries needed to resolve this question were not obtained until quite recently (Miller, Foukal and Keil 1984, Cavallini, Ceppatelli and Righini 1985).

Our line profile results for the two $g = 0$ FeI lines $\lambda 5434$ and $\lambda 4065$ are shown in Figure 3a. The two left panels show the line profiles observed in cell centers and in the network. The right two panels show the bisectors of the cell and network profiles at a scale expanded 40 times. All the bisectors show the characteristic "C" curvature (Dravins, Lindegren and Nordlund 1981), but the network bisector curvature is less than that of the cell bisector. Both the absolute curvature and the cell-network curvature are larger for $\lambda 5434$ than for $\lambda 4065$, which is formed over a narrower height (and velocity) interval.

We can see that if the relative position of the cell and network $\lambda 5434$ profiles were measured with a line-wing sensor such as a magnetograph, the network profile would appear shifted to the red by 100-200 msec^{-1} . But the cell and network bisectors coincide in the line core for both the lines shown here. This indicates that no relative velocity between cell and network is measured in that part of the line profile formed highest and thus least affected by the granulation I-V correlation.

Figure 3b from Miller, Foukal and Keil (1984) shows how the observed decrease of network line curvature can be simulated for atmospheres in which the effect of granular convection is decreased by specified amounts. The observed decrease can be produced, for instance, by a model in which roughly 20% of the network area is covered with flux tubes that completely inhibit granular convection. Figure 3c from Cavallini, Ceppatelli and Righini (1986) shows how closely the observed bisectors can be simulated with a more sophisticated model.

The close coincidence of the cell and network bisectors in the line cores shows that any general downflows present in the network must lie below the noise level of $+20 \text{ msec}^{-1}$ of our study. This limit on downflow velocity at supergranule cell edges is not low enough to rule out supergranulation as an overturning cell pattern. The continuity equation can still be satisfied (at least kinematically) if we suppose that the horizontal flow at $v_h \sim 0.5 \text{ km sec}^{-1}$ is confined to a thin layer comparable to the depth of photospheric line formation, with up- and downflows over large areas. However, it is questionable whether such a pattern would be dynamically realistic and stable. Unfortunately, there are no good dynamical models of supergranulation to use for guidance.

The $+20 \text{ msec}^{-1}$ limit we have placed on v_d is based on about 5 arc sec spatial resolution, so it does not rule out the possible existence of much larger downdrafts inside flux tubes occupying only a small fraction of the network area. Giovanelli and Slaughter (1978) were the first to use the technique of observing the position of the V Stokes profile which measures the degree of circular polarization, and thus is indicative of flows inside the flux tube. They found a red-shift indicating downflow of 0.6 kms^{-1} .

More recently, Stenflo et al. (1984) have observed the full Stokes V profile of network structures using the Fourier Transform Spectrometer at Kitt Peak. They find no evidence for a downflow, but they do note a pronounced asymmetry of the red and blue V profile intensities (Fig. 4), which could explain how the observations of Giovanelli and Slaughter (made by setting on the line wings with a magnetograph) might have indicated an apparent red-shift. More recent observations by S. Solanki and E. Wiehr indicate that a discrepancy between the results of Stenflo et al. and later observations of Wiehr (1985) have been resolved in favor of the observation of no downflows exceeding $+0.25 \text{ km sec}^{-1}$. The relatively large error on these observations is due to the large uncertainty in the absolute rest wavelength of the lines used, which is required as a reference for the zero-level crossing of the V Stokes profile.

The above discussion indicates that there is presently no direct observational evidence for downflows at supergranule edges, nor inside magnetic flux tubes. Another conclusion is that line-wing comparisons such as used in magnetographs are not well suited to measurement of small velocities of order 10 msec^{-1} in solar plasmas where line profile asymmetries can account for apparent shifts of several hundred meters sec^{-1} . It is helpful to use lines known to be relatively less susceptible to the I-V correlation, such as $\lambda 4065$. Alternatively, velocities can be measured through shifts in the line core (e.g., Kuhn 1983). Studies of line profiles with a spectrograph are required to check results.

IV. Dynamics of Spicules and Fibrils

Observations of spicules at the limb and their $H\alpha$ disc analogues seen as network rosettes and fibrils indicate that these structures are ubiquitous in solar magnetic regions, and their propulsion must be due to a rather general mechanism. The observations (see, e.g., Beckers 1972) indicate that we have a relatively cool ($\sim 10^4 \text{ K}$), dense ($\rho \sim 10^{-13} \text{ g cm}^{-3}$) plasma column propelled to a height of $7-10 \times 10^3 \text{ km}$ over 5-10 mins at a velocity of about $10-20 \text{ km sec}^{-1}$. It turns out that these deceptively simple requirements pose a dynamical problem which is not yet solved.

Following the work of Osterbrock (1961) most models have considered the spicule to be the more or less direct result of a pressure disturbance originating in the photosphere and propagating outward along the magnetic field lines. Since these field lines become force-free in the chromosphere, the problem reduces essentially to that of a shock tube at these altitudes. The most basic difficulty facing dynamical models is how to account for the rather high density at heights of up to 10^4 km, without producing high temperatures and flow velocities far in excess of the observed values. Since adiabatic shocks produce only modest compression, the density requirement at $h \sim 10^4$ km seems to require that the plasma of $\rho \sim 10^{-13}$ g/cm³ that is found at $h \sim 2000$ km in quiet sun models be propelled upwards by about 8000 km.

This problem has been studied in most detail by Suematsu et al. (1982) and Hollweg (1982). Their results are similar, and we describe them using figures from Suematsu et al. Figure 5a shows a 3-D representation of the upward propagation of the disturbance, and the response of the transition region. We see that as the disturbance moves through the transition region and on outwards into the corona, the cool material is propelled outward along ballistic trajectories (see also Fig. 5b), and eventually begins to fall back. A feature of these models are the rebound shocks that continue to be generated from the base of the atmosphere in response to the original disturbance. These successive shocks continue to lift the cool material to spicular heights.

The flaw in these interesting models is their adiabatic nature, which does not take into account the powerful dissipation that must decrease the amplitude of non-linear waves and shocks propagating through the upper photosphere and chromosphere. The importance of this dissipation is illustrated in Fig. 6a (from Ulmschneider 1971) for simple waves of flux density similar to that required for spicule excitation. We see that compressional waves of period below 50 secs used by Hollweg (1982) and by Suematsu et al. (1982) lose all but a tiny fraction of their flux by the time they have travelled to $h = 2000$ km.

We have calculated (Foukal and Smart 1981) the dissipation suffered by such shocks propagating along diverging field lines which will tend to decrease the losses, since the increasing area of the shock front reduces its energy flux density and thus its strength, which sensitively determines its dissipation rate. Our results are illustrated in Fig. 6b, and they show that although inclusion of this effect helps, the losses still remain very high.

The effect of including such radiative losses in the development of the specific disturbances responsible for the spicules of Hollweg (1982) and Suematsu et al. (1982) has recently been studied by Mariska and Hollweg (1986). The results of their adiabatic and non-adiabatic calculations are given for comparison in Fig. 7. We see that the adiabatic disturbance propagates with increasing amplitude past $h = 2000$ km, while in the non-adiabatic calculation, radiative losses rapidly damp the wave, so that essentially nothing remains at the transition region altitude. These results show the difficulty of attempting to explain spicules as the result of single or recurrent disturbances of high frequency propagating up from the photosphere.

The difficulty persists even if we consider isothermal shocks; i.e., associate the spicule with rapid cooling and condensation of thermally unstable coronal material behind a pressure disturbance. The problem then is to

cause sufficiently rapid radiative cooling behind the shock and produce upward propagation of the $T \sim 10^4$ K isotherm at $v \sim 10$ -20 km sec⁻¹. In unpublished calculations we have carried out, the medium was initially taken to be in energy equilibrium between inflow of heat by conduction from the corona above, and local radiative losses. The passage of a shock disturbs this balance by increasing the density and thus the radiative losses, and also by somewhat smoothing the temperature gradient. Both effects promote thermal instability, leading to upward propagation of the chromospheric isotherms, although actual mass motions are modest. We found that isotherm propagation speeds in the range 10-15 km sec⁻¹ may be achieved behind a strong $M_S = 4$ shock, but this shock is so highly dissipative that one must face the question of how a disturbance of that strength could ever have reached $h = 2000$ km from the photosphere.

In summary, we see that the highly dissipative nature of the upper photosphere and chromosphere make it difficult to understand how disturbances of sufficient amplitude to drive spicules and fibrils can reach the required heights. This is true whether we envisage the spicule to be caused by the quasi-adiabatic upward propulsion of the chromospheric isotherms, as did Osterbrock (1961) and most recently Hollweg (1982) and Suematsu et al. (1982), or whether we identify spicules with the upward propagation of a thermal instability into the corona, as is implicit in the isothermal shock case calculated by Wentzel and Solinger (1967) and was more explicitly studied in our calculation described above.

The main conclusion from the studies of spicule dynamics so far seems to be that some means of obviating the dissipation must be found, if the attractive concept of driving spicules directly by photospheric motion is to be preserved. One possibility is to consider disturbances of long period, so that energy can continue to be supplied to the "piston" to balance the large losses at the shock front that it is driving. A model in which the whole atmosphere is slowly lifted by deformation of the flux tube may be viable, but a consistent model needs to be constructed. Another approach is to simply trigger the spicule disturbance and supply the energy higher up, where radiative dissipation is less effective. A logical energy source might be reconnection, as suggested by Uchida (1969) and Pikelner (1969).

HRSO observations will no doubt contribute to resolution of these questions. The work of Dunn and Zirker (1973) on the photospheric sites of spicule and fibril formation is a good guide. Much might be done with continuous 0.1 arc second resolution in tracing spicule development through the atmosphere with filtergrams and spectra to study the morphology and kinematics of these fascinating and fundamental structures.

V. Coronal Loop Flows

Figure 11b shows an image of a post-flare loop observed at Big Bear on December 19, 1982. It clearly consists of many fine thin filaments, and analysis of its structure offers some test of the fundamental plasma scales that one might expect to resolve with a space telescope such as HRSO. Microdensitometric tracings we performed across the loop legs show H_α structures as thin as about 0.4". We have found that these are consistent with the scales and cross-sectional area filling factors derived from comparison in this same loop of various diagnostics of local density n_e and mean column density $n_e \ell$ obtained from line ratios, Stark effect and Thomson scattering

(Foukal, Hoyt and Gilliam 1986). Smaller scales down to the proton gyroradius of a few cm might well exist, but they are not demanded by these observations.

Time-lapse films show the development of cool condensations in this loop, and their proper motion down the field lines, on time scales of tens of minutes. There is no doubt that these proper motions in H_{α} represent flows, since we see clearly in Fig. 8 how a slit placed at a similar loop apex shows little relative Doppler shift of the condensations (seen here in H_{γ}), and increasing shift up to about 50 km sec^{-1} as the condensation picks up speed moving down the loop legs, when the slit is moved lower (Foukal 1978). Observations of this kind of flows in visible and UV radiations certainly convince us that the solar atmosphere is dynamical, and that advective transports probably dominate the energy balance equation. But attempts to construct models of these loop structures have not made much progress in answering the key questions--namely what process heats coronal loops, and what is the source of the mass excess that illuminates one set of field lines more than another?

To make faster progress, one might do better to confront the possible mechanisms with direct observational tests rather than proceeding by the circuitous route of constructing ever more complicated (and not very unique) atmospheric models. As an example of such an approach I would like to show some results obtained recently in a study of possible macroscopic electric fields in coronal loops. The presence (or absence) of detectable electric fields in post-flare loops bears directly upon both the energy balance and mass balance problems. Reconnection models used to explain dissipation of magnetic energy require the existence of an intense macroscopic E-field to allow relative motion of field lines and plasma at a slip rate given by $v_s = E \times B/B^2$. Intensities of order $E \sim 10\text{-}10^2$ volt/cm are quite likely. The reconnection also provides one mechanism by which plasma can cross magnetic field lines at the high rate v_s , a process of relevance in the mass balance problem along a given flux tube. Clearly then, inability to detect fields of this magnitude with a suitable diagnostic could directly test the importance of reconnection and at least one kind of cross-field plasma flow. On the other hand, measurement of the magnitude, orientation, etc., of E would be extremely helpful in improving our ideas of how this process operates in the corona.

Figure 9 shows the high Balmer lines in a bright post-flare loop, and a plot of their halfwidth against Balmer number. The rapid increase in width shows clear Stark effect corresponding to an electric field of order 10^2 volt/cm. This sort of broadening has been known for decades in flares and has been used as a diagnostic of high local plasma densities $n_e \sim 10^{12} \text{ cm}^{-3}$. The question is whether at least a good fraction of this total electric field might be due to macroscopic electric fields associated with reconnection or perhaps with waves.

To answer this question we need a remote sensing technique that will enable us to distinguish between macroscopic, ordered electric fields and the microscopic, disordered fields of pressure broadening. A new diagnostic for this purpose was recently described by Foukal, Hoyt and Gilliam (1986). As shown in Fig. 10a, the transverse Stark effect is very similar to the transverse Zeeman effect, except that the π components (polarized linearly along the E-field) now lie in the wings, and the σ (polarized linearly transverse to E) lie closer to the unshifted wavelength. This is the opposite of the Zeeman effect. By placing a polarizing prism before the spectrograph, we thus

see the maximum Stark broadening at the position θ_{\max} when its transmission axis is aligned with the π vibration direction, and a minimum broadening at the angle θ_{\min} at 90° to θ_{\max} . We expect then that if we take successive Balmer line spectra at different polarizer angles θ of a loop in which a uniform E-field is present with a substantial component in the sky-plane, the plots of $\Delta\lambda_{1/2}$ vs. n for the separate spectra should reveal a maximum broadening in the spectra taken at θ_{\max} , and a minimum at θ_{\min} (Fig. 10b).

Results of observations carried out so far on a bright post-flare loop using this method are shown in Fig. 11a. It can be seen that the curves for $0 \leq \theta \leq 45$ exhibit significantly larger slope for $n > 15$ than do the curves for $90 \leq \theta \leq 135$. This leads us to associate θ_{\max} (and thus the E-field direction) with an orientation corresponding to roughly radial in Fig. 11b. The field intensity required is approximately 10^2 volts cm^{-1} . The scale over which the field is detected is $L \sim 10^4$ km, but it might occupy only a small fraction of the volume, provided the emission measure is sufficient in the electrified plasma to dominate the Balmer line emission passed through the slit. The E-field observed must be uniform in space over a time scale of at least 10^3 secs.

The observed E-field direction is compatible with reconnection occurring either near the top or side of the loop, since $E = v_s \times B$. The magnitude of the field is about an order of magnitude larger than conventional models of flare loop reconnection (e.g., Somov and Titov 1985) would suggest. However, the fields could easily be much higher, since v_s is quite dependent on the local Alfvén speed and thus on the local density in the small reconnecting region.

For reasons given by Foukal, Hoyt and Gilliam, this result is unlikely to be caused by instrumental effects since three active prominences showed none of the ordering effect with θ seen in Fig. 11a. The result could be a statistical fluke, however, and more observations of this kind are needed. Observations of the high Balmer lines with a linear polarizer before the spectrograph slit might be profitably tried with the HRSO. The ability to resolve and track very small plasma elements might significantly increase the sensitivity to the electric fields of waves and reconnection, and study their spatial distribution and time dependence.

This work was supported under NSF grant ATM 8519121 and NASA contract NAS 5-29349.

References

- Athay, G. 1981, in "Solar Active Regions," F. Orrall, ed. Colorado Univ. Press, p. 83.
- Beckers, J. 1972, *Ann. Rev. Astr. Ap.* 10, 73.
- Beckers, J. 1977, *Ap. J.* 213, 900.
- Brueckner, G. 1981, in "Solar Active Regions," F. Orrall, ed. Colorado Univ. Press, p. 113.
- Cavallini, F., Ceppatelli, G., and Righini, A. 1985, *Astron. Ap.* 143, 116.
- Cavallini, F., Ceppatelli, G., and Righini, A. 1986, *Astron. Ap.* in press.
- Cook, J. 1985, in "Theoretical Problems in High Resolution Solar Physics," H. Schmidt, ed. Max Planck Institute Publication MPA 212, p. 308.
- Dravins, D., Lindegren, L., and Nordlund, A. 1981, *Astron. Ap.* 96, 345.
- Dunn, R. and Zirker, J. 1973, *Solar Phys.* 33, 259.
- Emslie, G. and Noyes, R. 1978, *Solar Phys.* 57, 373.
- Foukal, P. 1978, *Ap. J.* 223, 1046.
- Foukal, P., and Smart, M. 1981, *Solar Phys.* 69, 15.
- Foukal, P., Hoyt, C., and Gilliam, L. 1986, *Ap. J.* 303, 861.
- Gilman, P., and Foukal, P. 1979, *Ap. J.* 229, 1179.
- Giovanelli, R., and Slaughter, C. 1978, *Solar Phys.* 57, 255.
- Giovanelli, R. 1980, *Solar Phys.* 67, 211.
- Hollweg, J. 1982, *Ap. J.* 257, 345.
- Howard, R. 1972, *Solar Phys.* 24, 123.
- Kuhn, J. 1983, *Ap. J.* 264, 689.
- Mariska, J., and Hollweg, J. 1986, *Ap. J.* in press.
- Miller, P., Foukal, P., and Keil, S. 1984, *Solar Phys.* 92, 33.
- Moore, R. 1981, in "The Physics of Sunspots," L. Cram and J. Thomas, eds., Sac Peak Publication, p. 259.
- Osterbrock, D. 1961, *Ap. J.* 134, 347.
- Pikelner, S. 1969, *Astron. Zhurnal* 13, 259.

- Simon, G. and Leighton, R. 1964, Ap. J. 140, 1120.
- Somov, B., and Titov, V. 1985, Solar Phys. 95, 141.
- Stenflo, J., Harvey, J., Brault, J., and Solanki, S. 1984, Astron. Ap. 131, 333.
- Suematsu, Y., Shibata, K., Nishikawa, T., and Kitai, R. 1982, Solar Phys. 75, 99.
- Tanenbaum, A., Wilcox, J., Frazier, E., and Howard, R. 1969, Solar Phys. 9, 329.
- Uchida, Y. 1969, Publ. Astr. Soc. Japan 21, 128.
- Wentzel, D., and Solinger, A. 1967, Ap. J. 148, 877.
- Wiehr, E. 1985, Astron. Ap. 149, 217.
- Ulmschneider, P. 1971, Astron. Ap. 14, 275.



Fig. 1 Drawing of an active region made on October 5, 1871, from spectro-helioscope observations in H_{α} by A. Secchi.

ORIGINAL PAGE 1
OF POOR QUALITY

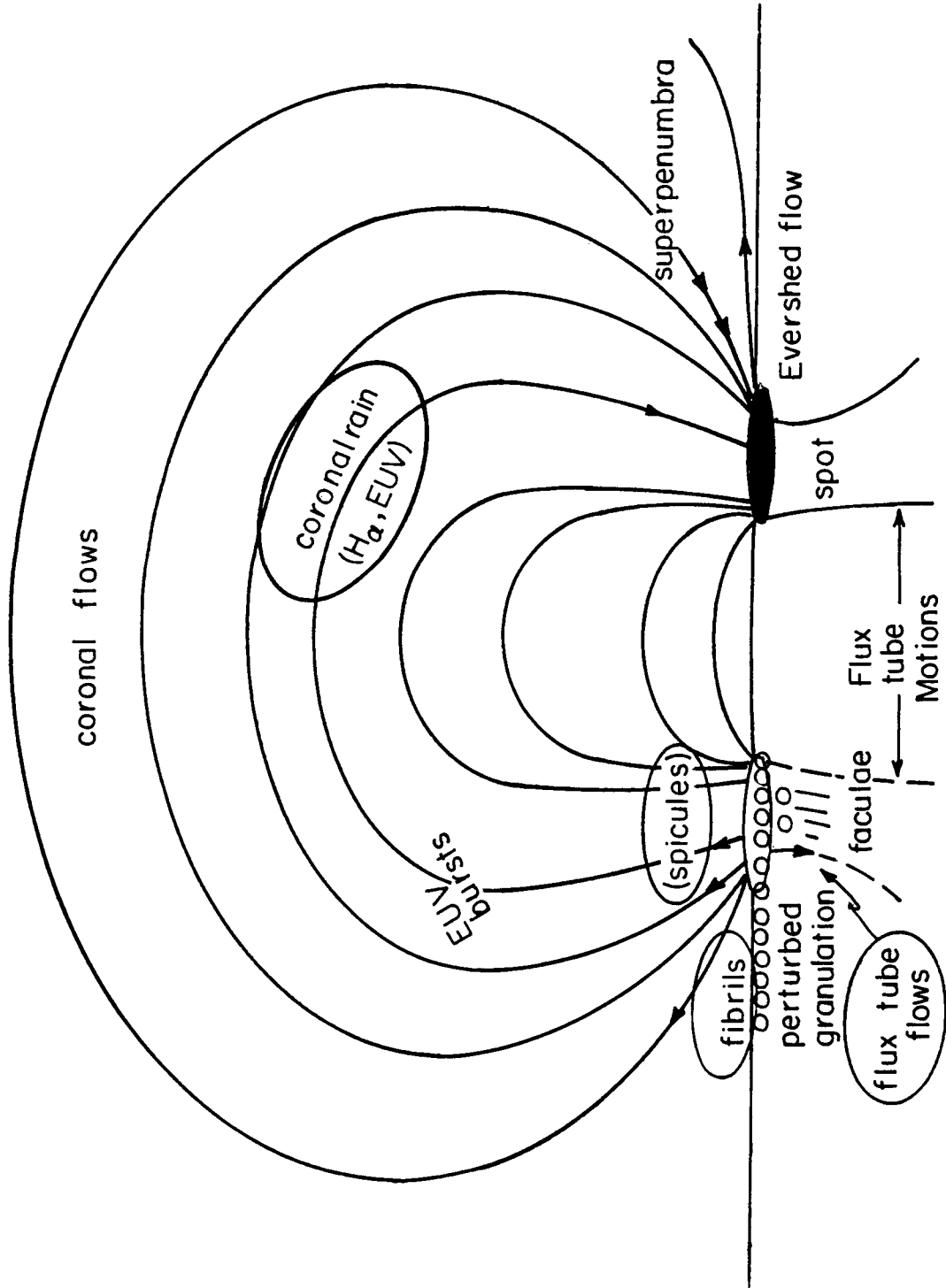


Fig. 2 Schematic representation of active region flows at photospheric, chromospheric and coronal levels.

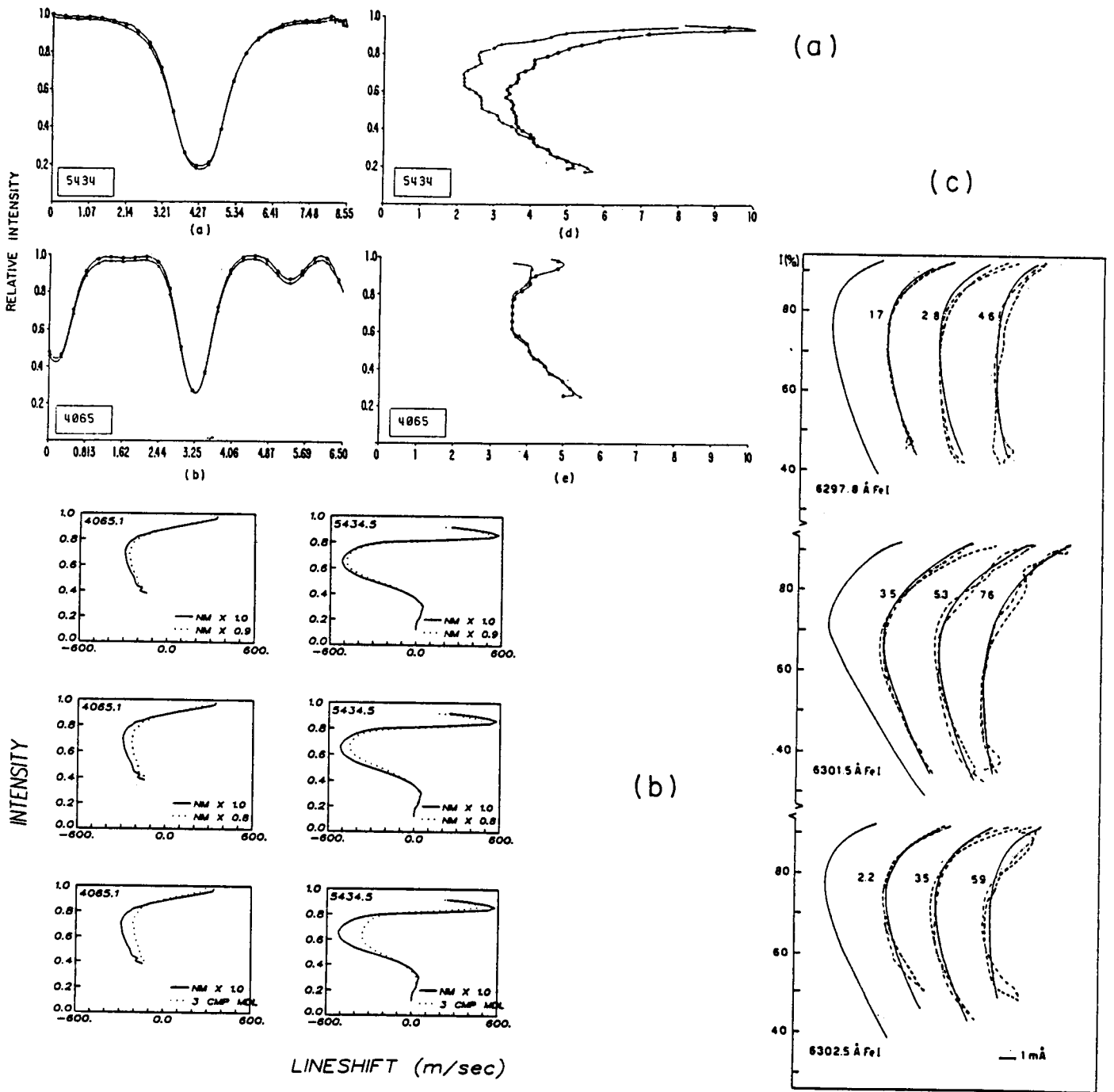


Fig. 3(a) Line profiles and bisectors for $\lambda 4065$, $\lambda 5434$ in cells (triangles) and network (circles). The abscissae are $\text{m}\text{\AA} \times 10^2$ for the profiles and $\text{msec}^{-1} \times 10^2$ for bisectors. The zeros are arbitrary.

(b) Line bisectors for $\lambda 4065$, $\lambda 5434$ computed for the Nelson-Musman (NM) granulation model (solid line), and for various degrees of convective inhibition.

(c) Observed (solid, left-hand line) and calculated bisectors for various scenarios using a three-component model consisting of normal granules, magnetic flux tubes, and non-convective atmosphere.

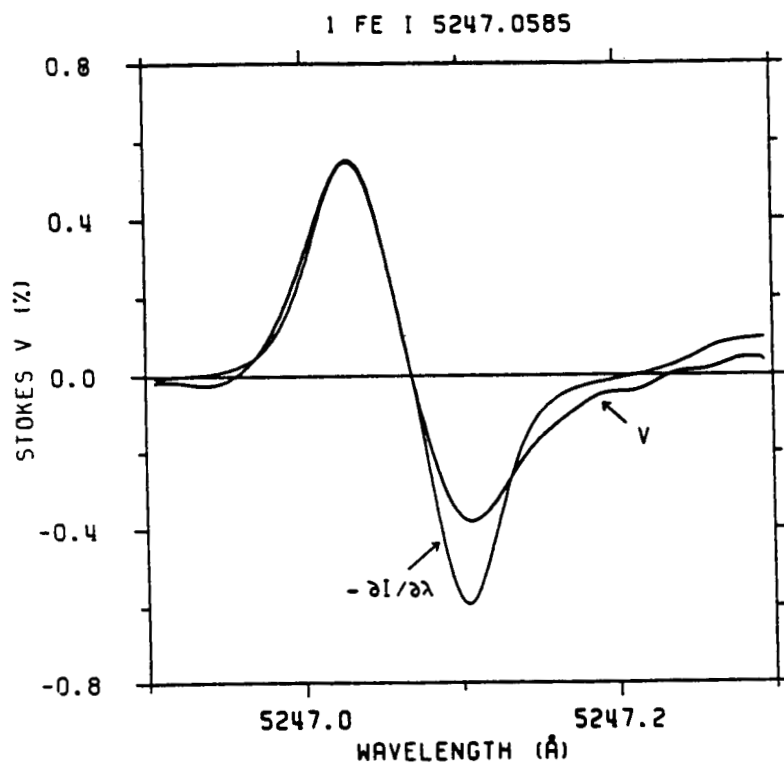


Fig. 4 Plot of the Stokes V profile (and also $dI/d\lambda$) for the FeI line 5247, showing the asymmetry of the blue and red V-profiles.

ORIGINAL PAGE IS
OF POOR QUALITY

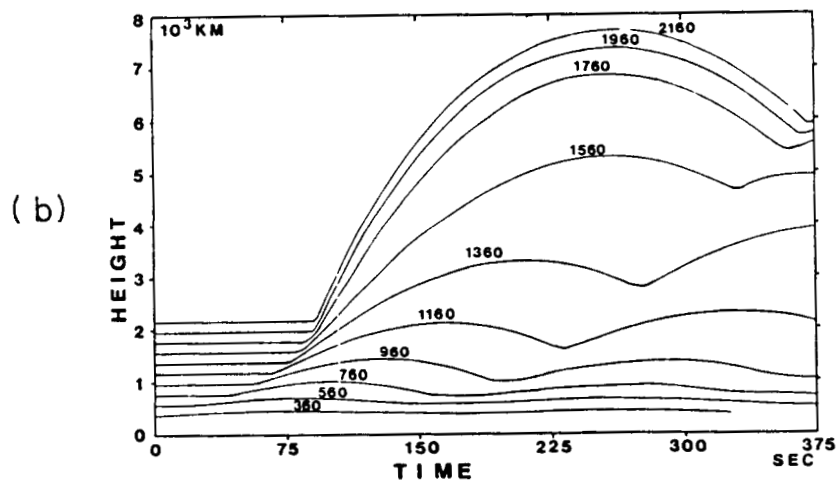
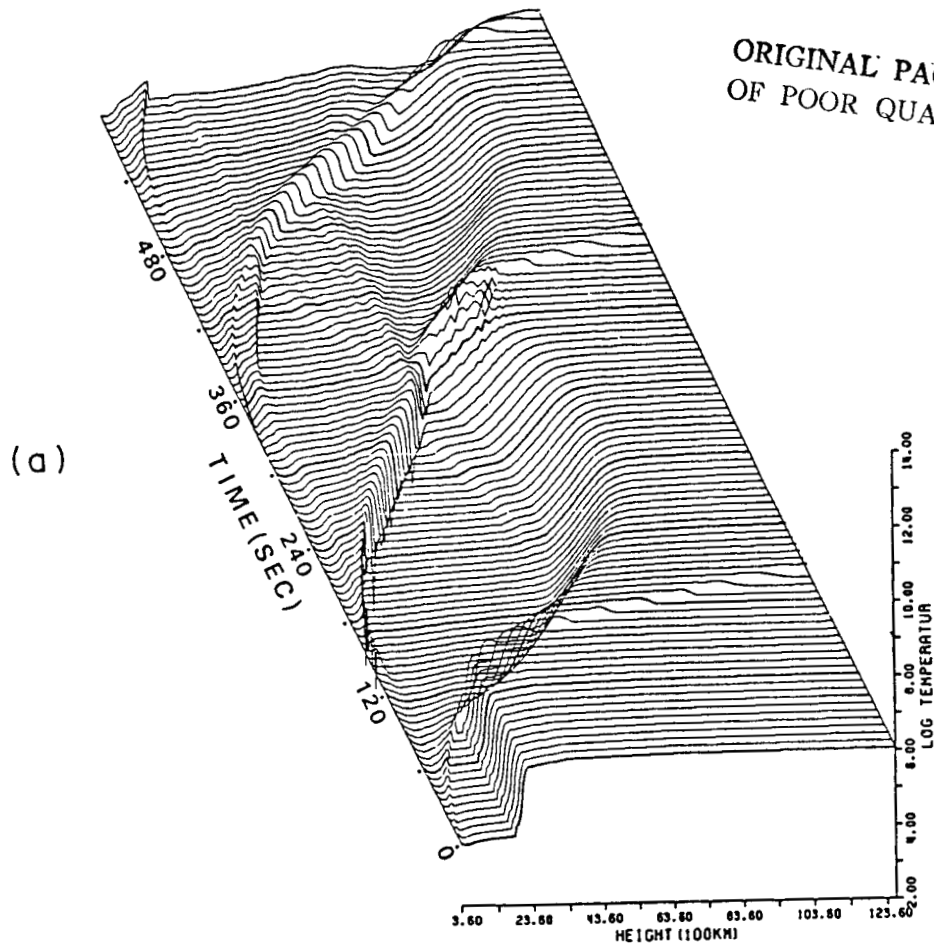


Fig. 5(a) Three-dimensional representation of upward propagating disturbances in the model of Suematsu et al. 1982. Coordinates are time (left), height (bottom) and log temperature (right). Successive traces are separated by ten seconds.

(b) Ballistic curves showing profiles of height with time, of material originating at heights marked (in km) on each curve.

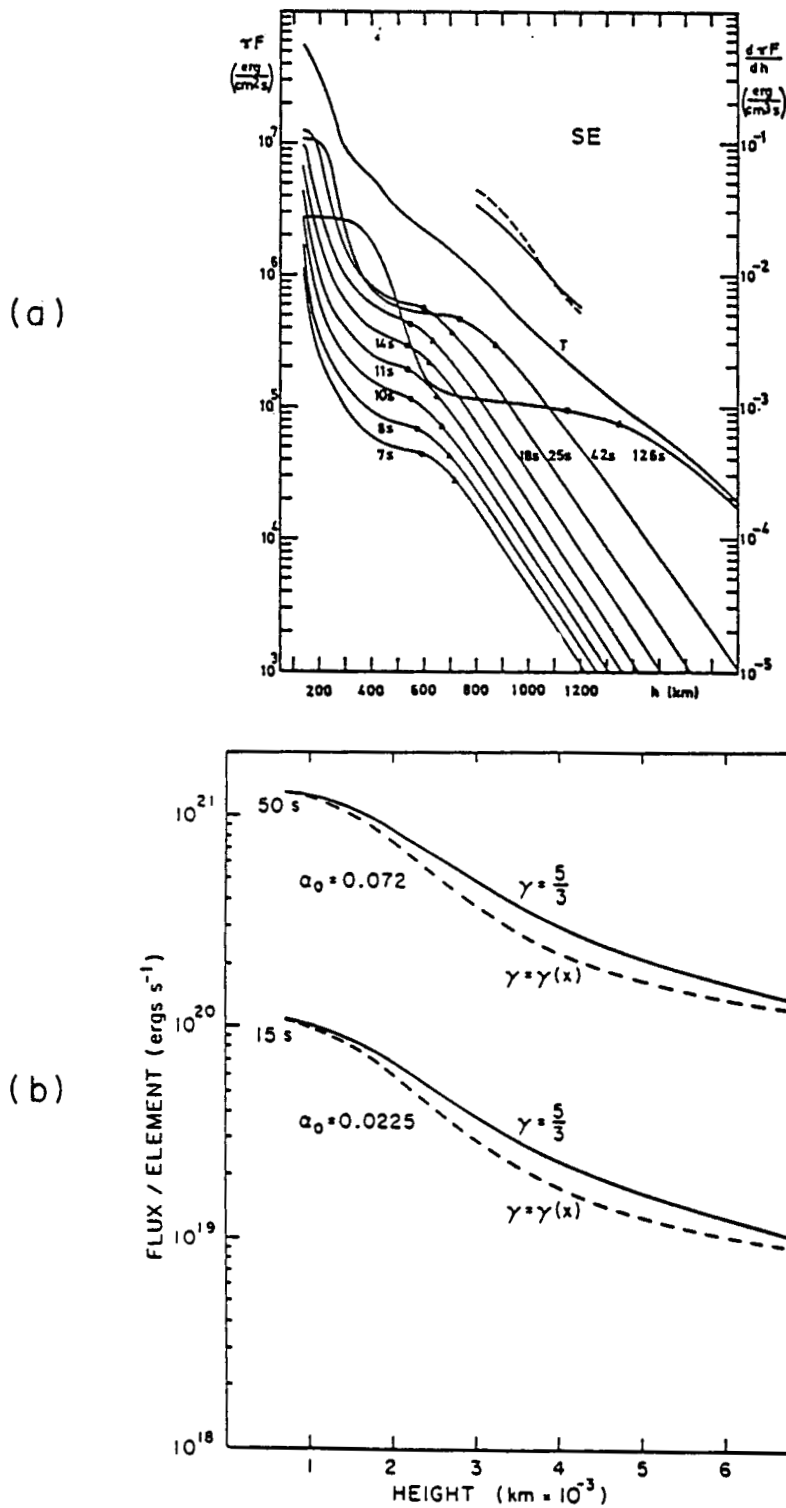


Fig. 6(a) Curves showing dissipation of flux in simple waves originating in the photosphere, between periods of 7 and 126s, for a plane-parallel atmosphere.

(b) Dissipation of flux for weak shocks in the upper photosphere and chromosphere, propagating along diverging field lines, for different γ , and for two values of shock strength $\alpha = M_S - 1$.

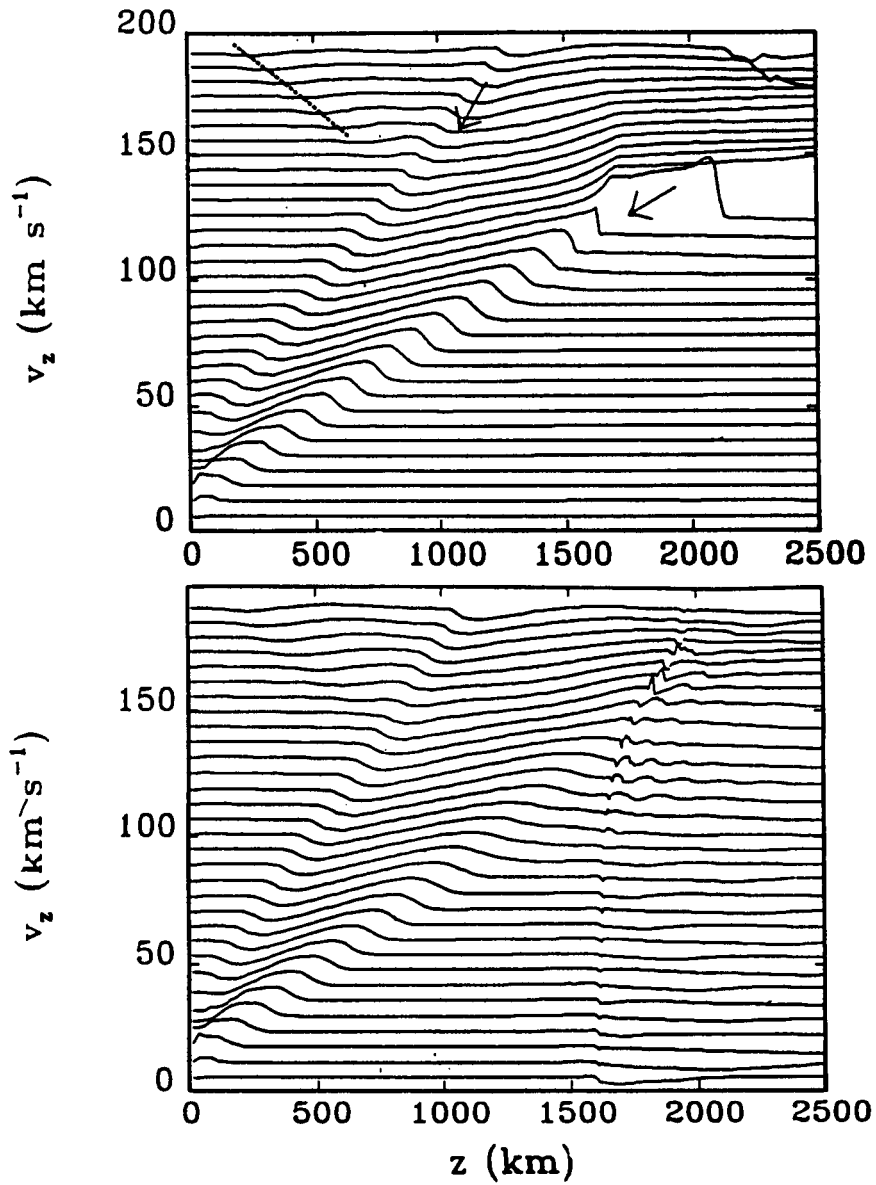


Fig. 7 Comparison of adiabatic (above) and non-adiabatic (below) calculations for the vertical velocity field v_z excited by successive compressional disturbances of identical initial amplitude and period. The glitches in the right-hand side of the lower frame are numerical errors.

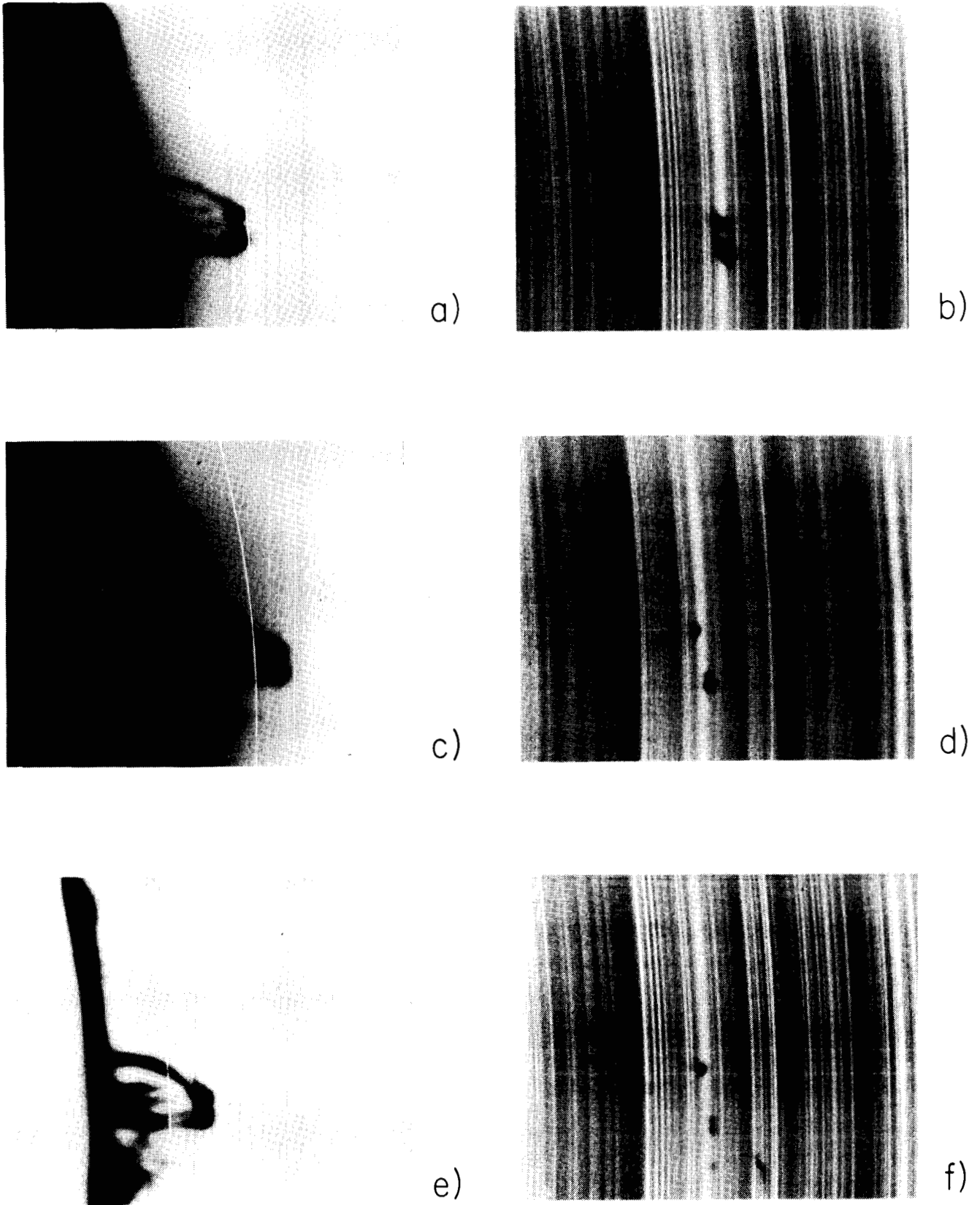


Fig. 8 Slit jaw pictures in H_{α} and spectra of H_{γ} for a post-flare loop. Note how the H_{γ} emission is increasingly Doppler separated as the slit is moved downward in the loop in frames a, c, e and (correspondingly) in spectra b, d, f.

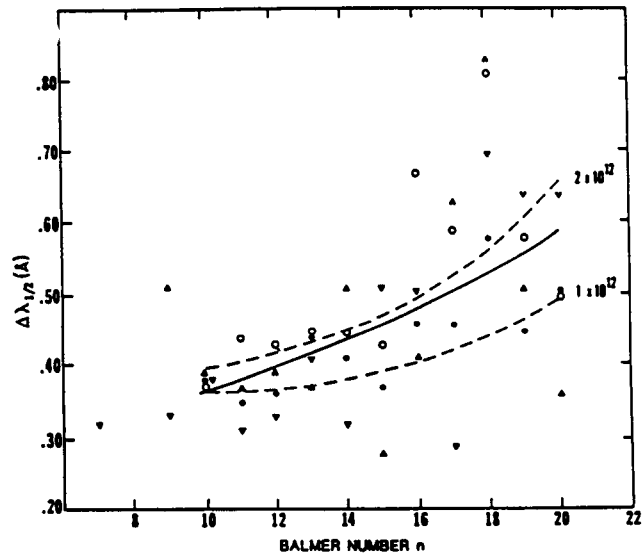
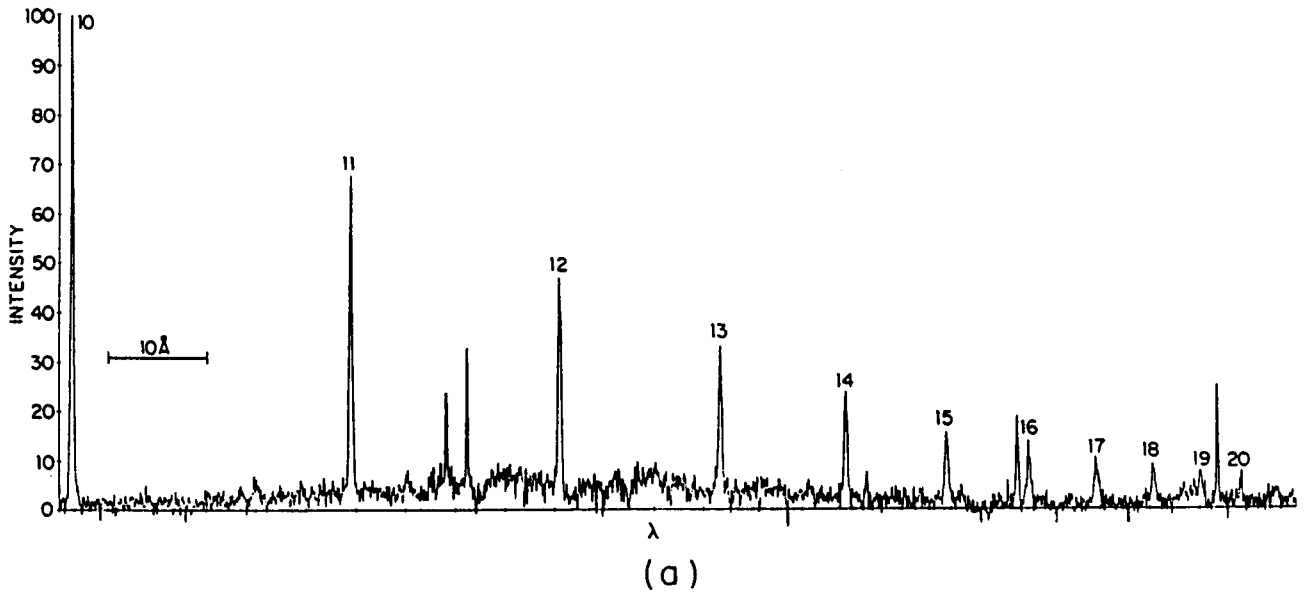


Fig. 9 The high Balmer lines in a post-flare loop (a) and (b) a typical plot of their half-width against Balmer number (from Foukal, Hoyt and Gilliam 1986).

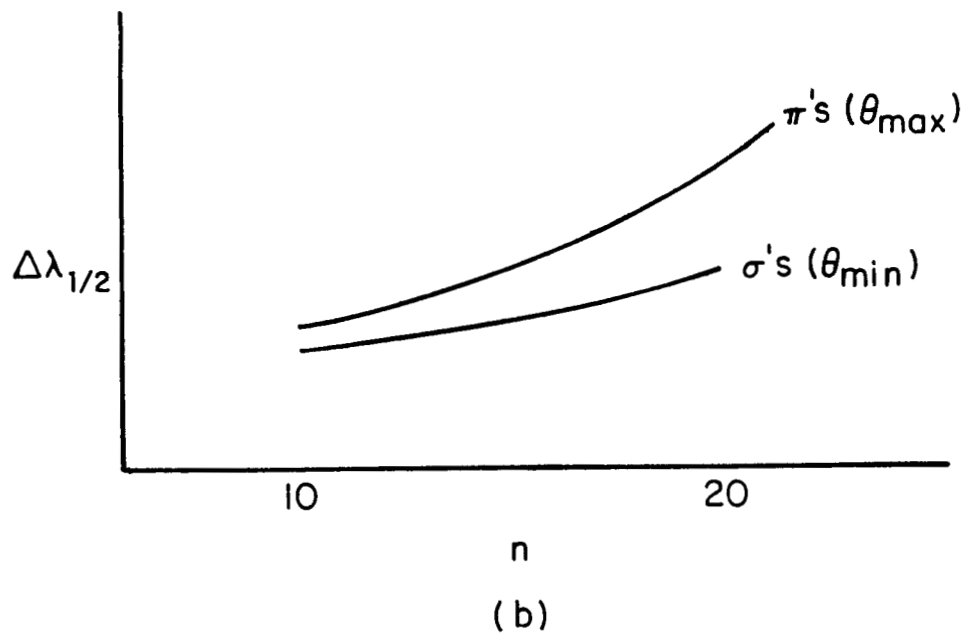
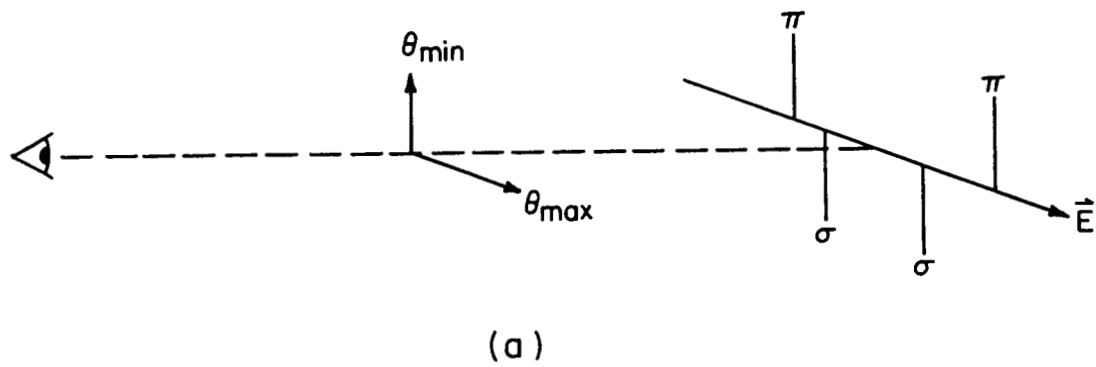
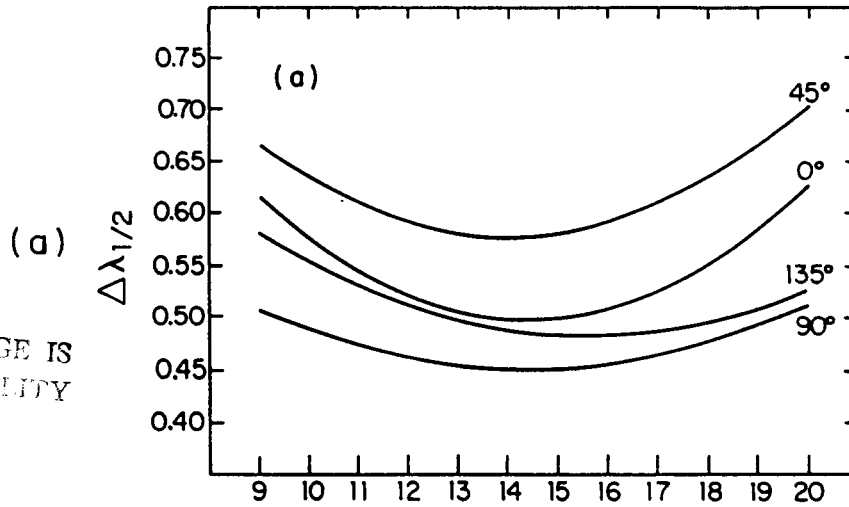


Fig. 10 Schematic diagram of the polarization structure of Balmer line Stark broadening (a) and the expected behavior of halfwidth plotted against Balmer number for π and σ components separately.

ORIGINAL PAGE IS
OF POOR QUALITY



(b)

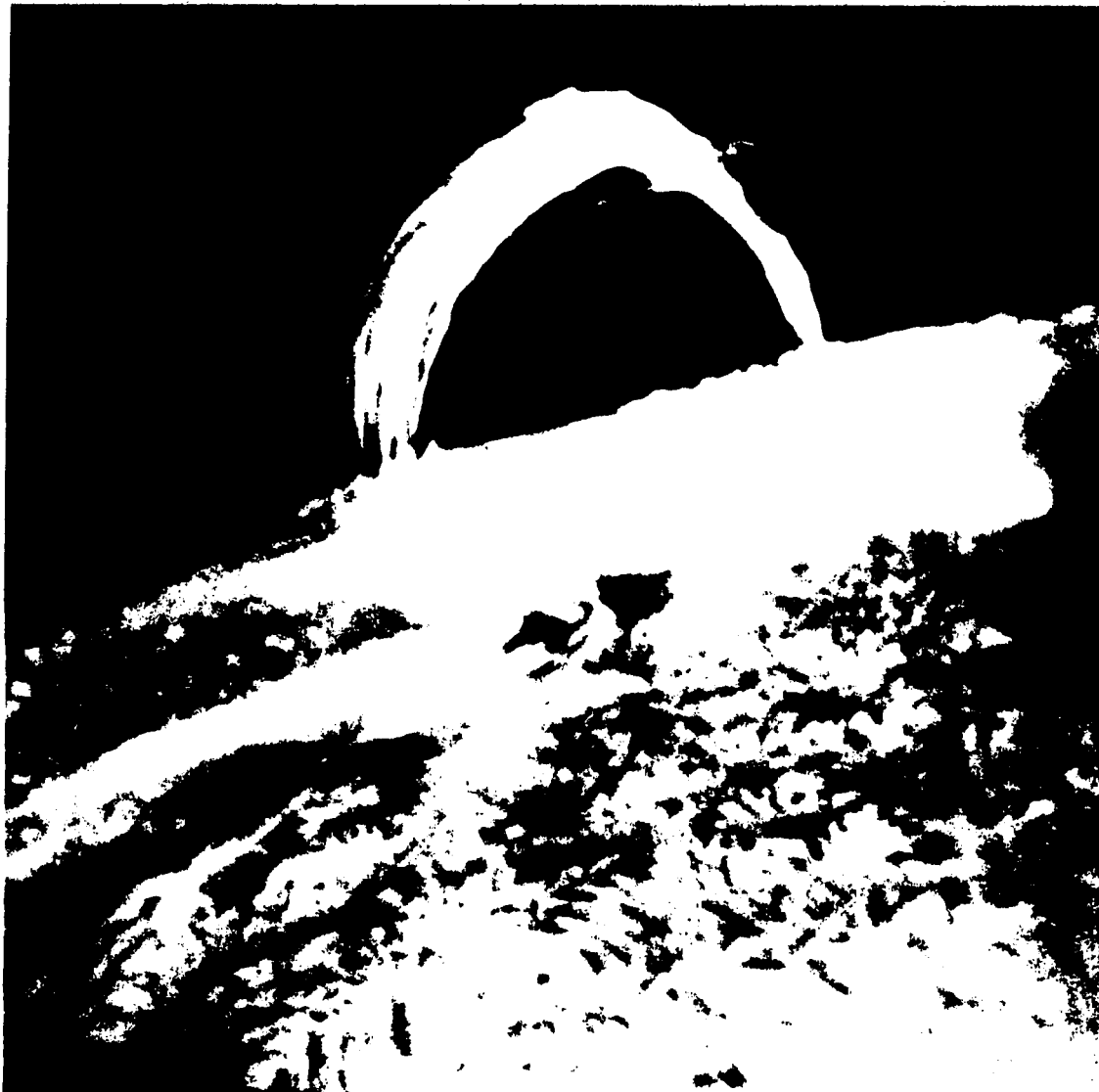


Fig. 11 Plots (a) of observed halfwidth against Balmer number for four different polarizer orientations, for the December 19, 1982, loop, shown in (b). The angle $\theta = 45^\circ$ corresponds roughly to E-field transverse to B-field at the loop apex.